VIII International Conference on Particle-Based Methods
PARTICLES 2023
U. Perego, M. Cremonesi, A. Franci (Eds)

THE EFFECT OF PARTICLE PROPERTIES ON BINARY MIXTURE SEGREGATION DURING BLAST FURNACE CHARGING

R. ROEPLAL, Y. PANG AND D. SCHOTT

TU Delft, Faculty of Mechanical Engineering
Mekelweg 2, 2628 CD Delft, The Netherlands
e-mail: r.n.roeplal@tudelft.nl

Abstract.
Segregation is likely to occur during blast furnace charging since the iron ore mixture contains particles differing simultaneously in size, shape and density. However, predicting how the mixture components will be distributed is particularly difficult due to the combined effect of these differences. Although the Discrete Element Method has been used extensively to gain understanding of segregation during blast furnace charging, most research has focused on simple mixtures in which particles differ only in size. In this work, we investigate how size, shape and density differences simultaneously affect mixture segregation in radial and vertical directions of a charged layer using the response surface methodology. We found that size and density difference between the mixture components significantly affect both radial and vertical segregation while shape differences, especially the aspect ratio, are relatively less important.

Keywords: Blast furnace, Binary mixture, Segregation, Sensitivity Analysis, DEM.

1 INTRODUCTION

A blast furnace is a counter-current reactor which produces liquid iron through a series of chemical reactions occurring between ascending reduction gases and a descending material bed which comprises alternating layers of coke and an ore mixture. The layered arrangement is achieved by sequentially charging the materials using a series of bulk handling equipment from the stock house until the rotating chute at the furnace top. It is well-known that segregation occurs during transportation through the charging apparatus, and an uneven distribution of the materials within the layers at the furnace top is therefore anticipated [1]. Layer segregation occurs in both radial and vertical directions, both of which can have a detrimental effect on the furnace permeability [1] and, consequently, the furnace efficiency.

Unlike the coke layers, the ore layers consist of particles differing simultaneously in size, shape and density. The complex interplay of these distinct property differences makes it difficult to predict the final ore layer homogeneity. For many years, the Discrete Element Method (DEM) has been used extensively to gain understanding of the segregation mechanisms during charging and the resulting material distribution [1]. However, most research in this regard is mostly focused on size segregation [2,3,4,5,6,7] while the effect of density difference has hardly been studied [8], and the effect of particle shape has not yet been considered. While a few studies have focused on mixtures of particles differing in both size and density [9,10,11], a comprehensive analysis involving size, density, and shape is currently lacking in the blast

furnace context. Moreover, segregation is typically analysed only in radial direction, so an analysis involving different layer directions is required.

In this work, we investigate how differences in size, shape and density affect segregation during binary mixture charging. We consider segregation in radial and vertical directions of the charged layer and determine which factors have the most significant effect on both responses using the response surface methodology (RSM). The novelty of this work is that, for the first time, we investigate the importance of all three material properties as well as their interactions on mixture segregation in multiple directions.

2 DEFINITION OF BINARY MXTURE PARAMETERS

Consider a mixture of two components (referred to as "particle type-1" and "particle type-2") differing simultaneously in size, density and shape. Given that both components are mono-sized, we define the size ratio of the mixture as

$$\tilde{d} = \frac{d_2}{d_1} \tag{1}$$

where d_1 and d_2 are the (equivalent) spherical diameters of particle type-1 and type-2, respectively. Similarly, we define the density ratio of the components as

$$\tilde{\rho} = \frac{\rho_2}{\rho_1} \tag{2}$$

Unlike particle size and density, particle shape cannot be defined by a single parameter. In order to systematically vary the particle shape, we use super-quadrics which are implicitly defined by [12]

$$\left[\left(\frac{x}{A}\right)^{2/e_1} + \left(\frac{y}{B}\right)^{2/e_1}\right]^{e_1/e_2} + \left[\frac{z}{C}\right]^{2/e_2} = 1 \tag{3}$$

where A, B and C are the semi-major axis lengths along x, y, and z directions, respectively, and e_1 and e_2 determine the particle roundness and sharpness of the particle edges. For simplicity, we consider only super-quadrics with $A = B$ and $e_1 = e_2 = e$. The aspect ratio (AR) is then defined as

$$AR = \frac{A}{C} = \frac{B}{C} \tag{4}$$

Given these parameters, the difference in shape between particle type-1 and type-2 is captured by

$$\widetilde{AR} = \frac{AR_2}{AR_1} \tag{5}$$

and

$$\tilde{e} = \frac{e_2}{e_1} \tag{6}$$

3 METHODS

DEM is used to simulate charging of binary mixtures of particles differing simultaneously in size, density and shape to a blast furnace with the same dimensions as the real industrial application. Next, RSM is used to investigate how $\tilde{d}$, $\tilde{\rho}$, $\widetilde{AR}$ and $\tilde{e}$ (the factors) affect the degree of segregation in terms of a segregation index (the response).

3.1 DEM Simulation

The basic principle of DEM can be expressed as follows: if all the forces and torques acting on a particle are known at each time step of the simulation, then its trajectory can be predicted in time using Newton's second law through numerical integration. Given the coarse, cohesionless nature of the raw materials during furnace charging, the total force acting on each particle is the sum of the gravitational force and interaction forces arising from the particle's contacts with surrounding objects. In this work, the Hertz-Mindlin no-slip contact model [13] is used to quantify the interaction forces. The material properties and contact model parameters for the binary mixture are summarized in Table 1. Since $\tilde{d}$, $\tilde{\rho}$, $\widetilde{AR}$ and $\tilde{e}$ are the factors in this investigation, the parameters of particle type-1 were kept constant and particle-type 2 was created based on the values of $\tilde{d}$, $\tilde{\rho}$, $\widetilde{AR}$ and $\tilde{e}$ in each simulation. The values of $\widetilde{AR}$ and $\tilde{e}$ outlined in experimental matrix (*cf.* Table 4) reveal that there were 9 distinct non-spherical shapes in this investigation, each in different sizes. To create these non-spherical particles with the required sizes in EDEM, we first generated shape templates (*.stl* files) in Matlab satisfying the values of $\tilde{d}$, $\tilde{\rho}$, $\widetilde{AR}$ and $\tilde{e}$ and subsequently fitted spheres to the templates in EDEM to form non-spherical clumps. The nine different shapes and fitted clumps are shown in Table 2.

Table 1. Model parameters used in this work. Abbreviations: P-P = particle-particle, P-W = particle-wall.

Parameter (symbol)		**Particle-type 1**	**Particle-type 2**
(Equivalent) spherical diameter (d)		0.014 m	*variable*
Aspect ratio (AR)		1	*variable*
Roundness/sharpness parameter (e)		1	*variable*
Particle density (ρ)		3015 kg/m^3	*variable*
Poisson's ratio (ϑ)		0.25	
Young's modulus (E)		2.5×10^7 Pa	
Restitution coefficient (e)	P-P	0.30	
	P-W	0.30	
Static friction coefficient (μ_s)	P-P	0.25	
	P-W	0.25	

Table 2. Shape templates and corresponding fitted clumps generated in EDEM.

Run 1-4	Run 5-8	Run 9-12	Run 13-16	Run 17-20 & Run 25	Run 21	Run 22	Run 23	Run 24
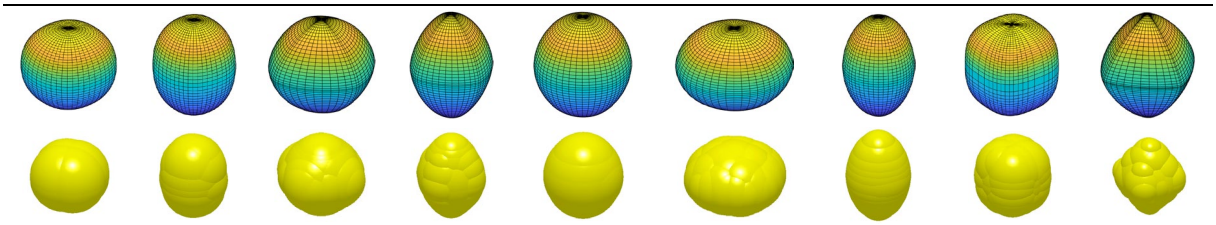								

The software package Altair EDEM 2022.2 was used on the DelftBlue high-performance cluster [14] with a single GPU (NVIDIA Tesla V100S-PCIE-32GB) to run simulations using the described models. A simplified charging setup (*cf.* Figure 1a) with true furnace dimensions was used, where charging starts at the chute inlet rather than from the hoppers. Two overlapping dynamic factories were used to generate the materials at a specific mass flowrate and velocity which are representative of actual blast furnace operation. Starting with an empty container, the mixture is distributed in rings as the chute rotates from the furnace walls towards the centre according to the actual charging programme used at TATA Steel Europe. At the end of the simulation, only particles in the analysis domain (*cf.* Figure 1b) are used for segregation analyses.

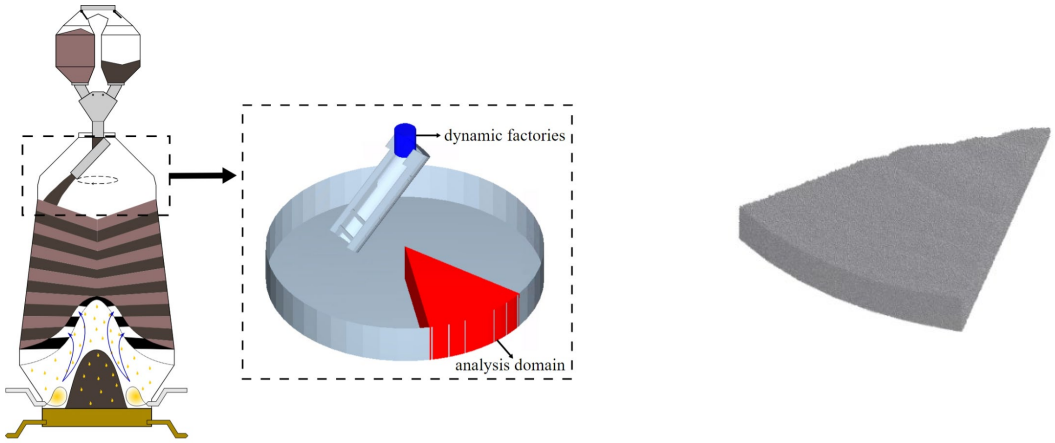

(a) (b)

Figure 1: Illustration of (a) the simplified simulation setup showing the overlapping dynamic factories (blue) and virtual analysis domain (red); (b) screenshot of the material bed inside the virtual analysis domain.

3.2 RSM experimental design

Factors and levels

The RSM is a statistical approach for determining the direct and interactive effects of process variables on the response parameters. Before applying RSM, it is necessary to choose an experimental design that will define which experiments should be carried out. In this work, we used RSM combined with a Central Composite Design (CCD) [15] to analyse the relationships between factors and responses. In the CCD, each variable is assigned five coded as $-\alpha$, -1, 0, $+1$ and $+\alpha$, where $\alpha = 2$ when using 4 factors. The factors and corresponding levels are summarized in Table 3.

Table 3. Factors and levels used in the Central Composite Design.

Parameter (Unit)	Coded variable	Range and levels				
		-2	-1	0	1	2
$\tilde{d}$ (-)	X_1	1.4	1.7	2.0	2.3	2.6
$\tilde{\rho}$ (-)	X_2	0.3	0.4	0.5	0.6	0.7
$\widetilde{AR}$ (-)	X_3	0.7	0.9	1.1	1.3	1.5
$\tilde{e}$ (-)	X_4	0.7	0.9	1.1	1.3	1.5

Responses

At the end of each simulation, the positions and volumes of type-1 and type-2 particles within the 45 degree analysis domain were extracted and subsequently imported to Matlab for segregation analyses. As we are dealing with a binary mixture, we used a segregation index based on tracer distribution [16]. First, the analysis domain was divided into a number of sub-domains (cells) and the mass fraction of particle type-1 (the tracer), x_1, in each cell was recorded. The segregation index was then calculated as the relative standard deviation of x_1:

$$SI = \sqrt{\frac{\sum_{i=1}^{N}\left(x_1^i - \overline{x_1}\right)^2}{N-1}} \tag{7}$$

where N is the number of sub-domains, $\overline{x_1}$ is the average mass fraction of all cells, determined by

$$\overline{x_1} = \frac{x_1^1 + \cdots + x_1^N}{N} \tag{8}$$

and x_1^i is the mass fraction of the tracer in the i-th cell determined by

$$x_1^i = \frac{m_1^i}{\left(m_1^i + m_2^i\right)} \tag{9}$$

where m_1^i and m_2^i are the mass of type-1 and type-2 particles in bin i, respectively. We quantified segregation in radial and vertical directions by dividing the analysis domain into equal-volume cells in the corresponding direction (*cf.* Figure 2), and subsequently calculating the segregation index (denoted as SI_r and SI_v for radial and vertical segregation, respectively). The SI values can range from 0.0 to 1.0, where 0.0 represents a perfectly mixed state and 1.0 represents a fully segregated state.

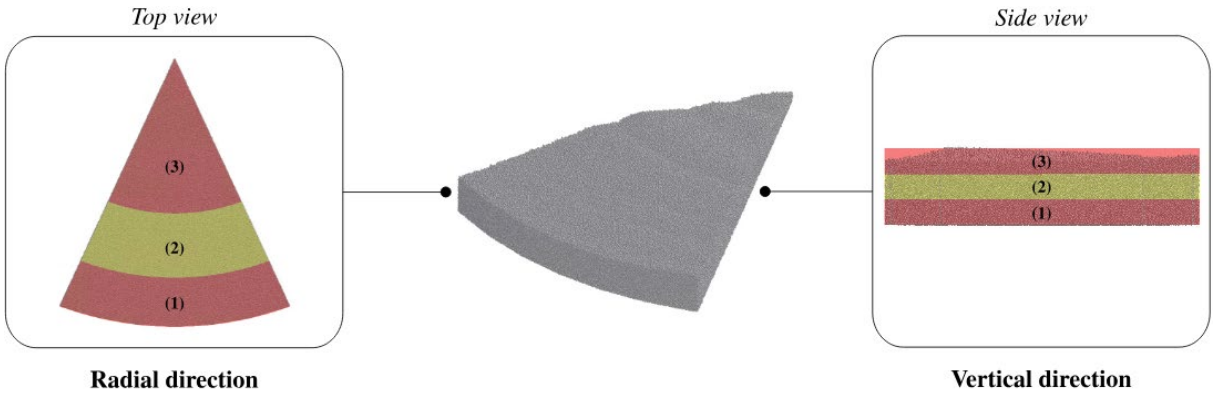

Figure 2: Illustration of domain decomposition into three equal-volume cells in radial and vertical directions.

Regression modelling and effects analysis

After running all simulations from the experimental matrix and calculating the responses, we used RStudio [17] to establish suitable regression models for SI_r and SI_v. Starting with a linear

model and sequentially adding second-order interactions, we determined the best fitting regression model using analysis of variance (ANOVA) of model coefficients. The ANOVA results were used to examine the importance of the factors and their interactions on SI_r and SI_v and contour plots were used to interpret effects.

4 RESULTS

4.1 Establishing response surface models

The results of the CCD are shown in Table 4 for radial and vertical segregation using 8 cells in radial direction and 4 cells in vertical direction. The reported SI values are the average of five replications for each run. The number of replications was selected by determining when the standard deviation of each run was below 10% of the average SI value.

Table 4. Results of the CCD where the reported SI-values are the average of three repetitions.

Run	Factors				Responses	
	X_1	X_2	X_3	X_4	SI_r	SI_v
1	-1	-1	-1	-1	0.021334	0.15811
2	+1	-1	-1	-1	0.027468	0.251526
3	-1	+1	-1	-1	0.019612	0.120574
4	+1	+1	-1	-1	0.026218	0.19901
5	-1	-1	+1	-1	0.020991	0.142938
6	+1	-1	+1	-1	0.027701	0.224824
7	-1	+1	+1	-1	0.014171	0.10299
8	+1	+1	+1	-1	0.021779	0.177688
9	-1	-1	-1	+1	0.029163	0.164868
10	+1	-1	-1	+1	0.037278	0.247862
11	-1	+1	-1	+1	0.016518	0.125226
12	+1	+1	-1	+1	0.019994	0.199684
13	-1	-1	+1	+1	0.030447	0.159084
14	+1	-1	+1	+1	0.036447	0.246568
15	-1	+1	+1	+1	0.016275	0.118826
16	+1	+1	+1	+1	0.019599	0.197216
17	-2	0	0	0	0.019267	0.102463
18	+2	0	0	0	0.027496	0.28185
19	0	-2	0	0	0.047823	0.207434
20	0	+2	0	0	0.024095	0.171552
21	0	0	-2	0	0.021173	0.167346
22	0	0	+2	0	0.020099	0.186633
23	0	0	0	-2	0.021132	0.168997
24	0	0	0	+2	0.026232	0.127473
25	0	0	0	0	0.023669	0.201732
26	0	0	0	0	0.024149	0.211928

Table 5 shows that, initially, full quadratic polynomial models best fit the data of Table 4 since they yield the best combination of R^2 and p-values. However, in both cases, the lack-of-fit value is below the recommended value. The insignificant terms of the full quadratic model were removed and, as shown in Table 5, the models were improved. The reduced quadratic models

for radial and vertical segregation are given by, respectively

$$SI_r = 0.0227 + 0.0027X_1 - 0.0052X_2 - 0.0005X_3 + 0.0015X_4 - 0.0028X_2X_4 + 0.003X_2^2 - 0.0009X_3^2 \quad (10)$$

and

$$SI_v = 0.19 + 0.042X_1 - 0.0178X_2 - 0.000057X_4 - 0.0109X_4^2 \quad (11)$$

Table 5. Summary of fit for different models: linear, two-factor interactions (2FI) and quadratic.

Source	Sequential p-value [1)]	Lack of Fit p-value [2)]	Multiple R^2	Adjusted R^2	Remark
Radial segregation					
Linear	7.574e-05	0.0083	0.6513	0.5879	
2FI	0.002125	0.0084	0.7596	0.6093	
Full Quadratic	7.941e-07	0.0452	0.9683	0.9313	Suggested
Reduced Quadratic	1.324e-10	0.137	0.9522	0.9336	Improved
Vertical segregation					
Linear	4.063e-09	0.06222	0.8605	0.8352	
2FI	2.966e-05	0.0460	0.8668	0.7836	
Full Quadratic	1.362e-05	0.08327	0.9482	0.8877	Suggested
Reduced Quadratic	2.458e-11	0.316	0.9221	0.9072	Improved

Guidelines [15]: [1)] $p < 0.05$, [2)] $p > 0.10$

4.2 Validation of response surface models

As a final validation step, we tested the developed regression models by conducting additional simulations which are within the design space but not included in the experimental matrix. As shown in Table 6, we performed two runs in which $\tilde{\rho}$ was varied ($X_2 = [-1\ 1]$) while keeping the remaining factors at zero coded level. It can be seen that there are relatively large differences between DEM and RSM predicted SI values. However, it must be noted that the DEM runs were not replicated. As we mentioned earlier in sec. 4.1, multiple replications are required in order to obtain a small confidence interval. Hence, for a more objective comparison, the DEM runs should be replicated and the RSM predicted SI values should be compared to a SI interval determined from DEM simulations.

Table 6. Comparison of DEM model and RSM model predictions for the degree of segregation as a function of the density ratio ($\tilde{\rho}$).

Run	Factor levels				Response: SI_r			Response: SI_v		
	X_1	X_2	X_3	X_4	DEM	RSM	Diff.	DEM	RSM	Diff.
1	0	-1	0	0	0.0346	0.0309	13.00%	0.255531	0.208384	18.5%
2	0	1	0	0	0.0198	0.0206	0.2%	0.157724	0.172856	9.6%

4.3 Effects analysis

Figure 3 shows the Pareto plots for standardized coefficients in the regression models. The plots provide insights into the relative importance of the different model predictors on SI_r and SI_v. The predictors with larger absolute standardized coefficients are more influential and the bars are coloured according to the direction of the relationship (positive/negative). The points on the cumulative proportion lines indicate how much of the total impact on the response variable is accounted for by including predictors in order of their importance. The plots indicate that X_2 ($\tilde{\rho}$) and X_1 ($\tilde{d}$) have the most significant effect on radial and vertical segregation, respectively. The shape factor X_3 ($\widetilde{AR}$) is of relatively less importance for SI_r, since the cumulative proportion line gradually levels off after the X_4 ($\tilde{e}$) predictor. Similarly, X_4 is much less important for SI_v.

Figure 4 and Figure 5 show the response surface plots for SI_r and SI_v, respectively. Figure 5a indicates that for a fixed shape ($X_3 = X_4 = 0$, which is nearly spherical) segregation in radial and vertical directions is reduced for lower values of X_1 and higher values of X_2. Considering the values of the factors in Table 3, this means that a reduction of segregation is achieved when the particles in the mixture have similar volumes (sizes) and densities. Xu et al. [8] found a similar result in their study of binary mixture charging. They considered a mixture of small and large (spherical) particles and kept the density of the small particles fixed at 2800 kg/m^3. They varied the density of the large particles from 1400 to 4200 kg/m^3 and found that radial segregation decreased as the density was reduced. This relationship is also observed for vertical segregation in Figure 6a. The symmetric nature of the surface plots in Figure 5b, d and f demonstrate the weak interaction of X_3 with other factors. The same can be seen for X_4 in Figure 6b and c. Radial segregation is always reduced for high and low values of X_3, so when the non-spherical particle is either flat or elongated. Vertical segregation is always reduced for low and high values of X_4, so when the particle shape deviates from significantly from spherical. The latter does not hold for radial segregation due the $X_2 - X_4$ interaction.

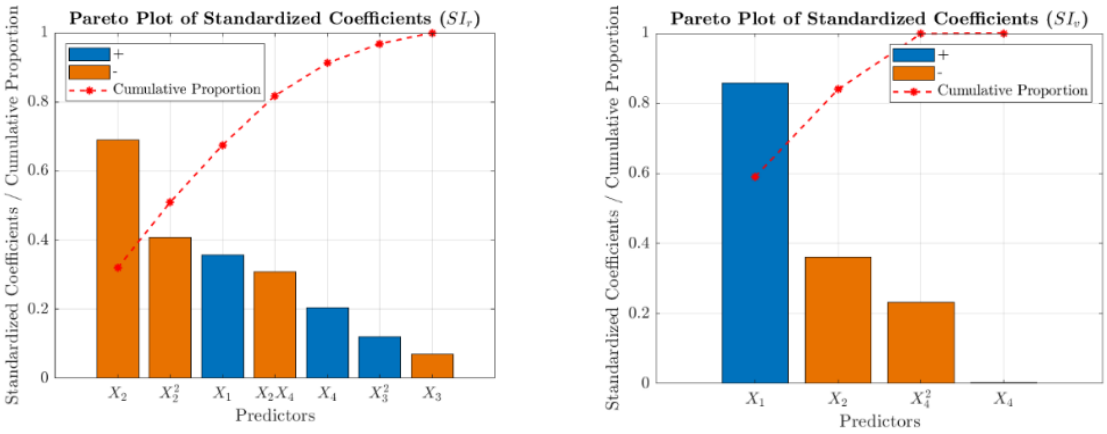

(a) (b)

Figure 3: Pareto plots for standardized coefficients in the regression models for (a) SI_r and (b) SI_v.

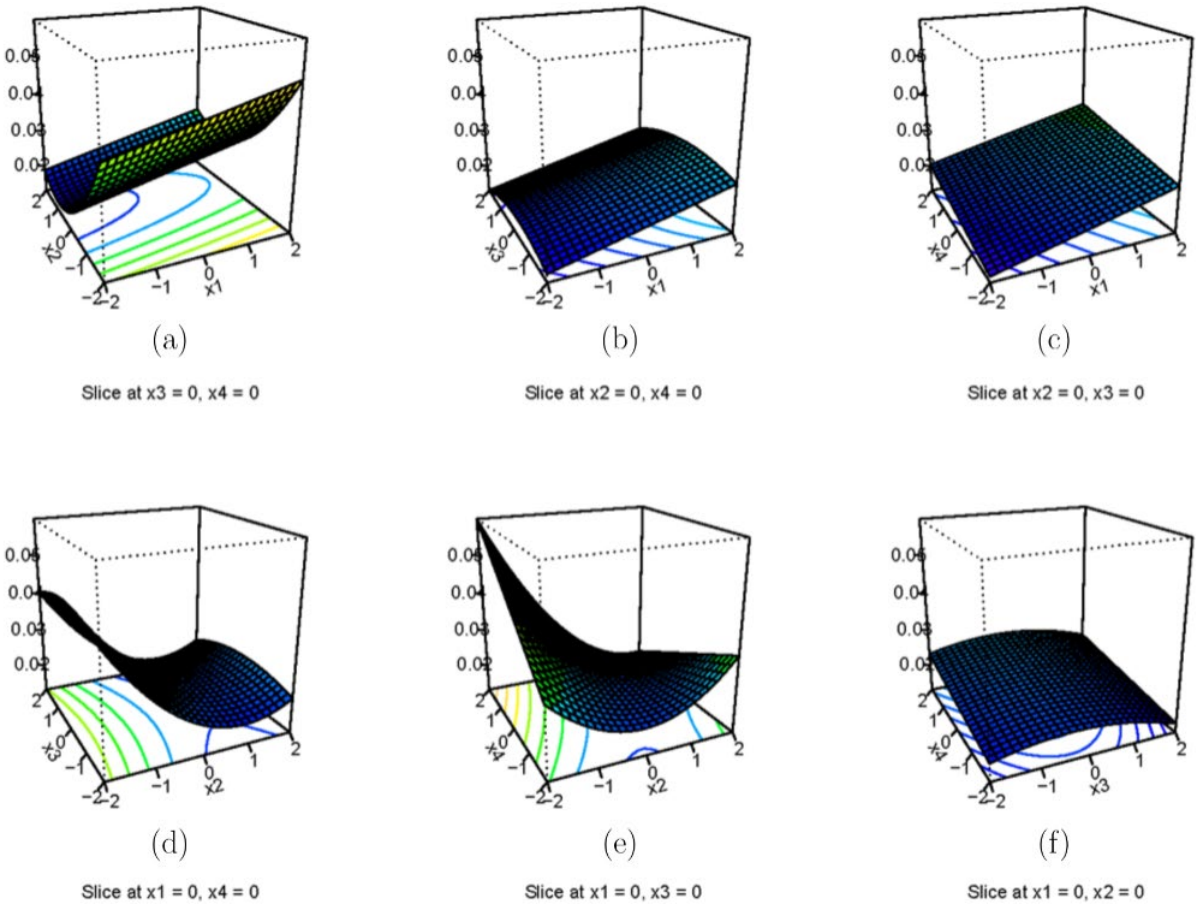

Figure 4: Response surface plots for SI_r.

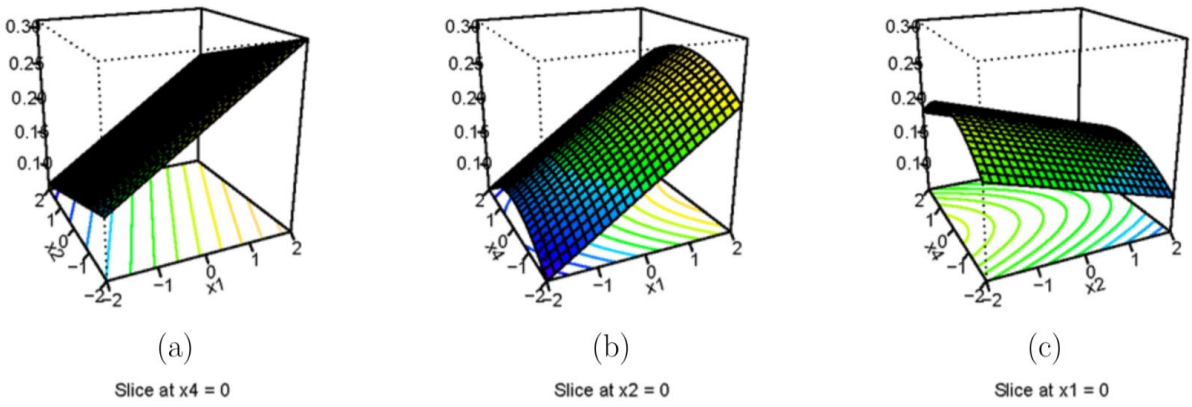

Figure 5: Response surface plots for SI_v.

5 CONCLUSION

The goal of this work was to investigate how size, density and shape differences between particles in a binary mixture simultaneously affect blast furnace segregation using the response surface methodology. The main findings of this work are as follows:

- Size and density differences are the most significant factors for both radial and vertical segregation, while shape differences have relatively less effect.
- Segregation in both radial and vertical directions decreases as the binary mixture components have equal volumes and densities. The non-spherical particle should be either flat or elongated to reduce radial segregation and the shape should differ significantly from a sphere to reduce vertical segregation.

In the future this work can be extended by including a factor which describes the particle size distribution of each of the components, making the results more applicable to actual industrial mixtures.

ACKNOWLEDGEMENT

This work was carried out as part of the "Industrial Dense Granular Flows" project, which received funding from the Dutch Research Council (NWO) in the framework of the ENW PPP Fund for the topsectors and from the Ministry of Economic Affairs in the framework of the "PPS-Toeslagregeling".

REFERENCES

[1] R. Roeplal, Y. Pang, A. Adema, J. van der Stel and D. Schott, *Modelling of phenomena affecting blast furnace burden permeability using the Discrete Element Method (DEM) – A review,* vol. 415, 2023, p. 118161.

[2] J. Zhang, J. Qiu, H. Guo, S. Ren, H. Sun, G. Wang and Z. Gao, "Simulation of particle flow in a bell-less type charging system of a blast furnace using the discrete element method," *Particuology,* vol. 16, pp. 167-177, 2014.

[3] W. Xu, S. Cheng, Q. Niu and G. Zhao, "Effect of the Main Feeding Belt Position on Burden Distribution during the Charging Process of Bell-less Top Blast Furnace with Two Parallel Hoppers," *ISIJ International,* vol. 57, no. 7, pp. 1173-1180, 2017.

[4] H. Wei, W. Ding, Y. Li, H. Nie, H. Saxén, H. Long and Y. Yu, "Porosity distribution of moving burden layers in the blast furnace throat," *Granular Matter,* vol. 23, 11 2021.

[5] H. Mio, Y. Narita, K. Nakano and S. Nomura, "Validation of the Burden Distribution of the 1/3-Scale of a Blast Furnace Simulated by the Discrete Element Method," *Processes,* vol. 8, no. 1, 2020.

[6] C. X. Li, K. J. Dong, S. D. Liu, G. R. Chandratilleke, Z. Y. Zhou and Y. S. Shen, "DEM study of particle segregation in the throat region of a blast furnace," *Powder Technology,* vol. 407, p. 117660, 2022.

[7] Z. Di, M. Huang, X. Zhou, J. Liu, J. Sun, P. Wang and H. Wang, "The influence of central coke charging mode on the burden surface shape and distribution of a blast furnace," vol. 21, no. 2, pp. 169-179, 2023.

[8] Y. Xu, K. Ma, C. Sun, Z. Liao, J. Xu, L. Wen and C. Bai, "Effect of Density Difference on Particle Segregation Behaviors at Bell-Less Top Blast Furnace with Parallel-Type Hopper," *9th International Symposium on High-Temperature Metallurgical Processing,* pp. 391–399-391–399, 2018.

[9] W. Xu, S. Cheng, Q. Niu, W. Hu and J. Bang, "Investigation on the uneven distribution of different types of ores in the hopper and stock surface during the charging process of blast furnace based on discrete element method," *Metallurgical Research & Technology,* vol. 116, p. 314, 1 2019.

[10] W. Xu, S. Cheng and C. Li, "Effect of the charging sequence of iron-bearing burden on burden distribution during the charging process of blast furnace based on discrete element method," *Ironmaking & Steelmaking,* vol. 0, no. 0, pp. 1-9, 2021.

[11] Z. Zhao, H. Saxén, Y. Liu, X. She and Q. Xue, "Numerical study on the influence of pellet proportion on burden distribution in blast furnace," *Ironmaking & Steelmaking,* pp. 1-8, 11 2022.

[12] H. Chen, S. Zhao and X. Zhou, "DEM investigation of angle of repose for super-ellipsoidal particles," *Particuology,* vol. 50, pp. 53-66, 2020.

[13] R. D. Mindlin, "Compliance of Elastic Bodies in Contact," *Journal of Applied Mechanics,* vol. 16, no. 3, pp. 259-268, 4 2021.

[14] (DHPC), Delft High Performance Computing Centre, *DelftBlue Supercomputer Phase 1,* Delft, 2022.

[15] Douglas C. Montgomery, Design and Analysis of Experiments, 8th ed., New York: John Wiley & Sons, 2013.

[16] A. Hadi, R. Roeplal, Y. Pang and D. L. Schott, "DEM Modelling of Segregation in Granular Materials: A Review," *KONA Powder and Particle Journal,* vol. advpub, pp. -, 2023.

[17] R Core Team, "R: A Language and Environment for Statistical Computing," 2021. [Online]. Available: https://www.R-project.org/.